Epidemiology of human culture: parietal rock art requires high population density

Authors: Richard Walker[*†1], Anders Eriksson*[†2], Camille Ruiz[3], Taylor Howard Newton[1], Francesco Casalegno[1]

Affiliations :

[1] Blue Brain Project, Ecole Polytechnique Fédérale de Lausanne, Switzerland

[2] Department of Medical and Molecular Genetics, Kings College, London, UK

[3] Ateneo de Manila University, Manila, The Philippines

[†]Joint first authors

[*]Correspondence: email: richard.walker@epfl.ch, anders.eriksson@kcl.ac.uk

Abstract: Demographic models of human cultural evolution have high explanatory potential but weak empirical support. Here we use climate-based estimates of ancient population densities and a global dataset of rock art sites to test an epidemiological model, where the spread of an innovation requires population density beyond a critical threshold. The model has stronger empirical support than a null model where rock art distribution and population density are independent. Tests for different areas and periods, and with independent population estimates, yield qualitatively similar results, supporting the robustness of the model. We conclude that a minimum population density is a necessary condition for the spread of rock art. Similar methods could be used to test the model for other artefacts and to compare it against other models.

One Sentence Summary: Combining climate-based estimates of ancient population densities with data for the global distribution of rock art over the last 46,000 years, we provide robust evidence that the diffusion of rock art requires population densities above a critical threshold.

It is widely accepted that the complexity and diversity of human cultures are a result of Cumulative Cultural Evolution (CCE), enabled by humans' unique neuroanatomy, and cognitive capabilities, especially their skills in "cultural learning" (*1–3*) . However, there is no evidence that variations in brain size and morphology explain any aspect of cultural patterning over the last 45,000 years (*4–6*). Against this background, demographic models of CCE (*7*) assign a determining role to population size, density and structure. Such models suggest that larger, denser, better connected populations produce more, innovations than smaller ones (*8*), are less vulnerable to stochastic loss of unique skills (*9*, *10*), and are more capable of exploiting beneficial transmission errors during social learning (*11*). They also suggest that well-connected metapopulations produce faster cultural innovation than metapopulations with weaker connections among sub-populations (*12*) .

Demographic models could potentially provide valuable explanations for spatiotemporal patterning in the global archaeological record. Their assumptions and conclusions are, however, hotly contested (*13–15*). Empirical studies are sparse and inconclusive, with a few supporting the role of demography e.g. (*11*, *12*, *16*, *17*), while others find no evidence for such a role (*18*, *19*). The majority use data on historical hunter-gatherer populations. Here, for the first time, we test a demographic model of cultural evolution against detailed data for prehistoric populations. Specifically, we test the ability of the model to predict the global, spatiotemporal distribution of parietal rock art sites over the last 46,000 years.

CCE involves the inception, diffusion and selective retention of cultural innovations – in this study, rock art. The model tested here (see Fig 1), inspired by SIR models in epidemiology (*20–22*),

focuses on diffusion, treated as analogous to the spread of a disease. The underlying assumption is that without diffusion, a localized innovation is unlikely to leave a trace in the archaeological record.

Consider the emergence of rock art in a metapopulation comprising N subpopulations or communities, where *I* and S are respectively the proportion of *infected* communities (communities that have adopted the innovation), and the proportion of *susceptible* communities (communities that have not). The innovation spreads from infected to susceptible communities at rate β. By analogy with empirical findings in (*23*) (see below), opportunities for transmission (contacts between communities) are proportional to the square root of population density. Infected communities *recover* (here: lose the ability to produce rock art) at rate γ.

In this model (see Fig 1 and SM Methods), there is a critical population density:

$$\rho^* = \left(\frac{\gamma}{\beta}\right)^2$$

such that

$$I^* = \begin{cases} 0, \rho \leq \rho^* \\ 1 - \sqrt{\frac{\rho^*}{\rho}}, \rho > \rho^* \end{cases}$$

where I^* is the final proportion of infected communities in a given area. The value of $\rho^*$is determined by the balance between γ and β, with lower values of γ and higher values of β associated with lower values. Below ρ^*, there are no infected communities; above ρ^*, I^* is an increasing function of population density.

I^* is not directly observable in the archaeological record. To test our model, we consider *site detection rates* i.e. the small probability, P, that a territorial cell of defined area contains at least one recorded instance of rock art. Since the proportion of cells where geology, climate and research effort allow the creation, preservation and recording of rock art is small, we write

$$P \cong \zeta\, I^*\, \rho$$

where ζ reflects the joint effects of these factors (see SM). The model predicts that for $\rho \leq \rho^*$, detection rates will be zero and that at higher densities it will rise in direct proportion to ρ. As a result, median population density for cells containing sites will be automatically higher than for the complete set of cells.

To test these predictions, we collated a dataset containing the locations, dates and characteristics of 133 scientifically dated rock art sites (see Methods, SM Table 1). Ancient population densities were estimated by combining data from two published models, informed by global genetic variation, and climate-based estimates of Net Primary Productivity (*24*, *25*) (SM - Methods). Population densities were inferred for all cells containing rock art site ("sites") and for all inhabited cells ("globals"). We then computed site detection rates (number of sites/number of globals) as a function of population density for all latitudes between 20-60N and 10-40°S, and all dates more recent than 46000 years ago - the only latitudes and dates with significant numbers of sites in our sample (119 sites) (see Fig. 2)

As predicted, sites were concentrated in cells with higher population densities; cells with lower densities contained very few sites (median population densities: sites: 29.92/100km^2; globals 15.31/100km^2). Using a Bayesian statistical framework, we estimated the most plausible parameter values for the model given the empirical observations (Fig. 3A). Posterior distributions for model parameters were tightly constrained (see SM Fig. 1) The inferred population density threshold for the model with the highest likelihood, was 13.18 individuals/100km^2 (95% CI: 6.66 -17.00). Comparison against a proportional model (site frequency directly proportional to population density) and a constant model (equal site frequency at all population densities) strongly supported rejection of the alternative models (see SM Table 1).

Seven sites in the rock art dataset were located in cells with inferred population densities below the density threshold inferred from the model. Since the dating for some of the sites in our dataset was problematic, we repeated our analysis using only sites with exact dates, obtained with direct methods. With this filtered dataset (55 sites), median population density for sites was higher than for globals (sites: 30.25; globals 15.31) and empirical support for the epidemiological model was again much stronger for the epidemiological model than for alternative models. The inferred value of the population density threshold (14.50 individuals/100km^2, 95% CI: 7.95-17.89) was close to the previous estimate (see SM Table 2).

Another potential source of errors was the model used to generate our population estimates. We therefore repeated our analyses using more recent population estimates (*26*), based on a different

climate model and different assumptions (see SM Materials and Methods). As in the earlier analysis, empirical support for the epidemiological model was much stronger than for the alternative null or proportional models. The CI for the inferred population density threshold (95% CI: 13.80-22.15) overlapped with the CI for the original analysis (see Fig. 3B, SM Table 2)

The scope of our study did not allow us to perform a comprehensive survey of the vast rock art literature. Large geographical areas in Central/South America, Central Africa, East and South-East Asia are practically unrepresented in our dataset (see Fig. 2A). Moreover, 60.9% of the sites in our full dataset, date from less than 10,000 years ago, and only 3.8% from before 40,000 years ago (see Fig. 2B). All this suggests the possibility of systematic bias. Suggestions that the literature itself is biased by ecological and taphonomic factors and by geographical variations in research effort (*27*) make the presence of such biases even more plausible.

To test their potential impact, we repeated our analysis for data from two culturally unrelated geographical areas (France-Spain and Australia) and for two distinct periods (from the present until 10,000 years ago, and from 10,000 until 46,000 years ago (SM Materials and Methods). In the case of France-Spain, the predicted effects were attenuated by high estimated population densities even in areas with no sites. Nonetheless, here too, as in the other three cases, we found higher median population densities for sites than for globals, stronger support for the epidemiological model than for alternative models and evidence for a threshold effect (SM Table 2). These findings *within* specific periods and geographical areas are evidence that our results are not due to *between* period or *between* area biases.

Another potential problem is the use of population density as a proxy for contacts between subpopulations. Grove has pointed out that individual contact numbers in hunter-gatherer populations depend not just on population density but also on mobility (*23*) – a finding that plausibly applies also to intercommunity contacts. To avoid this objection, the model incorporates Grove's empirical finding that mobility among modern hunter-gatherers is inversely proportional to the square root of population density. This is not, however, an essential feature. Changes in the precise form of this relationship would change the predicted value of the critical threshold for a given population density. However, the predictive power of the current version suggests that the relationship used in our analysis is a good approximation to reality.

To summarize, our study models one of the key mechanisms required for CCE ("diffusion"), and tests the predictions of the model for the case of parietal rock art. In all our analyses, (Fig. 3B, SM Table 2), median population densities for sites (25.03-30.43 individuals/km^2) are consistently higher than for the corresponding globals. In all cases, analysis empirical support for the epidemiological model and its predicted threshold effect is much stronger than for alternative proportional or null models. Taken together, these results provide robust grounds to reject the null hypothesis that the emergence of rock art is unrelated to demography, and strong support for the epidemiological model.

Importantly, nothing in our model or empirical results suggests that a minimum level of population density is a *sufficient condition* for the emergence of rock art. In fact, there are many areas of the

globe (e.g. in equatorial Africa) with high population densities and little or no reported rock art. We conjecture that creation, preservation and discovery of rock art depends on a multitude of factors, including those posited by the demographic models reviewed in the introduction to this article. The epidemiological model should be seen as complementary to these models.

One important feature of our study is the use of population density as the key independent variable, avoiding the need to measure the size of "culturally effective populations" (*9*), a construct which is difficult to operationalize where populations' geographical range is unknown. A second one is the choice of "detection frequency" rather than "cultural complexity" as the dependent variable. These methodological features will facilitate the application of our model and methods outside the case of rock art and in contexts where other constructs are difficult to measure.

Our rock art dataset, population estimates, and software tools are publicly available at https://github.com/rwalker1501/cultural_epidemiology.git. Other researchers are encouraged to use them to replicate our findings, to test our hypotheses for other classes of artifact and with other population estimates, and to explore their own models.

References

1. M. Tomasello, *The Cultural Origins of Human Cognition* (Harvard University Press, 2009).

2. J. Henrich, *The Secret of Our Success: How Culture Is Driving Human Evolution, Domesticating Our Species, and Making Us Smarter* (Princeton University Press, 2015).

3. K. N. Laland, *Darwin's Unfinished Symphony: How Culture Made the Human Mind* (Princeton University Press, 2018).

4. S. McBrearty, A. S. Brooks, The revolution that wasn't: a new interpretation of the origin of modern human behavior. *J. Hum. Evol.* **39**, 453–563 (2000).

5. F. d'Errico, C. B. Stringer, Evolution, revolution or saltation scenario for the emergence of modern cultures? *Philos. Trans. R. Soc. B Biol. Sci.* **366**, 1060–1069 (2011).

6. E. M. Scerri, M. G. Thomas, A. Manica, P. Gunz, J. T. Stock, C. Stringer, M. Grove, H. S. Groucutt, A. Timmermann, G. P. Rightmire, Did our species evolve in subdivided populations across Africa, and why does it matter? *Trends Ecol. Evol.* (2018).

7. S. Shennan, in *Emerging Trends in the Social and Behavioral Sciences* (John Wiley & Sons, Inc., 2015; http://onlinelibrary.wiley.com/doi/10.1002/9781118900772.etrds0073/abstract).

8. M. Kremer, Population growth and technological change: one million B.C. to 1990. *Q. J. Econ.* **108**, 681–716 (1993).

9. S. Shennan, Demography and cultural innovation: a model and its implications for the emergence of modern human culture. *Camb. Archaeol. J.* **11**, 5–16 (2001).

10. L. S. Premo, S. L. Kuhn, Modeling effects of local extinctions on culture change and diversity in the Paleolithic. *PLoS One*. **5**, e15582 (2010).

11. J. Henrich, Demography and cultural evolution: How adaptive cultural processes can produce maladaptive losses - The Tasmanian case. *Am. Antiq.* **69**, 197–214 (2004).

12. A. Powell, S. Shennan, M. G. Thomas, Late Pleistocene demography and the appearance of modern human behavior. *Science*. **324**, 1298–1301 (2009).

13. M. Collard, K. Vaesen, R. Cosgrove, W. Roebroeks, The empirical case against the 'demographic turn'in Palaeolithic archaeology. *Phil Trans R Soc B*. **371**, 20150242 (2016).

14. K. Vaesen, M. Collard, R. Cosgrove, W. Roebroeks, Population size does not explain past changes in cultural complexity. *Proc. Natl. Acad. Sci.* **113**, E2241–E2247 (2016).

15. J. Henrich, R. Boyd, M. Derex, M. A. Kline, A. Mesoudi, M. Muthukrishna, A. T. Powell, S. J. Shennan, M. G. Thomas, Understanding cumulative cultural evolution. *Proc. Natl. Acad. Sci.* **113**, E6724–E6725 (2016).

16. M. A. Kline, R. Boyd, Population size predicts technological complexity in Oceania. *Proc. R. Soc. B Biol. Sci.*, rspb20100452 (2010).

17. M. Collard, A. Ruttle, B. Buchanan, M. J. O'Brien, Population size and cultural evolution in nonindustrial food-producing societies. *PloS One*. **8**, e72628 (2013).

18. M. Collard, M. Kemery, S. Banks, Causes of toolkit variation among hunter-gatherers: a test of four competing hypotheses. *Can. J. Archaeol. Can. Archéologie*, 1–19 (2005).

19. M. Collard, B. Buchanan, M. J. O'Brien, Population size as an explanation for patterns in the Paleolithic archaeological record. *Curr. Anthropol.* **54**, S388–S396 (2013).

20. R. Ross, An application of the theory of probabilities to the study of a priori pathometry. Part I. *Proc. R. Soc. Math. Phys. Eng. Sci.* **92**, 204–230 (1916).

21. W. O. Kermack, A. G. McKendrick, A contribution to the mathematical theory of epidemics, in *Proceedings of the Royal Society of London* (The Royal Society, 1927; , vol. 115, pp. 700–721.

22. H. W. Hethcote, Three basic epidemiological models in *Applied Mathematical Ecology*, S. A. Levin, T. G. Hallam, L. J. Gross, Eds. (Springer Berlin Heidelberg, Berlin, Heidelberg, 1989; https://doi.org/10.1007/978-3-642-61317-3_5), *Biomathematics*, pp. 119–144.

23. M. Grove, Population density, mobility, and cultural transmission. *J. Archaeol. Sci.* **74**, 75–84 (2016).

24. A. Eriksson, L. Betti, A. D. Friend, S. J. Lycett, J. S. Singarayer, N. von Cramon-Taubadel, P. J. Valdes, F. Balloux, A. Manica, Late Pleistocene climate change and the global expansion of anatomically modern humans. *Proc. Natl. Acad. Sci.* **109**, 16089–16094 (2012).

25. M. Raghavan, M. Steinrucken, K. Harris, S. Schiffels, S. Rasmussen, M. DeGiorgio, A. Albrechtsen, C. Valdiosera, M. C. Avila-Arcos, A.-S. Malaspinas, A. Eriksson, I. Moltke, M. Metspalu, J. R. Homburger, J. Wall, O. E. Cornejo, J. V. Moreno-Mayar, T. S. Korneliussen, T. Pierre, M. Rasmussen, P. F. Campos, P. d. B. Damgaard, M. E. Allentoft, J. Lindo, E. Metspalu, R. Rodriguez-Varela, J. Mansilla, C. Henrickson, A. Seguin-Orlando, H.

Malmstrom, T. Stafford, S. S. Shringarpure, A. Moreno-Estrada, M. Karmin, K. Tambets, A. Bergstrom, Y. Xue, V. Warmuth, A. D. Friend, J. Singarayer, P. Valdes, F. Balloux, I. Leboreiro, J. L. Vera, H. Rangel-Villalobos, D. Pettener, D. Luiselli, L. G. Davis, E. Heyer, C. P. E. Zollikofer, M. S. Ponce de Leon, C. I. Smith, V. Grimes, K.-A. Pike, M. Deal, B. T. Fuller, B. Arriaza, V. Standen, M. F. Luz, F. Ricaut, N. Guidon, L. Osipova, M. I. Voevoda, O. L. Posukh, O. Balanovsky, M. Lavryashina, Y. Bogunov, E. Khusnutdinova, M. Gubina, E. Balanovska, S. Fedorova, S. Litvinov, B. Malyarchuk, M. Derenko, M. J. Mosher, D. Archer, J. Cybulski, B. Petzelt, J. Mitchell, R. Worl, P. J. Norman, P. Parham, B. M. Kemp, T. Kivisild, C. Tyler-Smith, M. S. Sandhu, M. Crawford, R. Villems, D. G. Smith, M. R. Waters, T. Goebel, J. R. Johnson, R. S. Malhi, M. Jakobsson, D. J. Meltzer, A. Manica, R. Durbin, C. D. Bustamante, Y. S. Song, R. Nielsen, E. Willerslev, Genomic evidence for the Pleistocene and recent population history of Native Americans. *Science*. **349**, aab3884–aab3884 (2015).

26. A. Timmermann, T. Friedrich, Late Pleistocene climate drivers of early human migration. *Nature*. **538**, 92–95 (2016).

27. R. G. Bednarik, The pleistocene art of Asia. *J. World Prehistory*. **8**, 351–375 (1994).

28. R. White, R. Mensan, R. Bourrillon, C. Cretin, T. F. G. Higham, A. E. Clark, M. L. Sisk, E. Tartar, P. Gardère, P. Goldberg, J. Pelegrin, H. Valladas, N. Tisnérat-Laborde, J. de Sanoit, D. Chambellan, L. Chiotti, Context and dating of Aurignacian vulvar representations from Abri Castanet, France. *Proc. Natl. Acad. Sci.* **109**, 8450–8455 (2012).

29. M. García-Diez, D. L. Hoffmann, J. Zilhão, C. de las Heras, J. A. Lasheras, R. Montes, A. W. G. Pike, Uranium series dating reveals a long sequence of rock art at Altamira Cave (Santillana del Mar, Cantabria). *J. Archaeol. Sci.* **40**, 4098–4106 (2013).

30. C. González-Sainz, A. Ruiz-Redondo, D. Garate-Maidagan, E. Iriarte-Avilés, Not only Chauvet: dating Aurignacian rock art in Altxerri B Cave (northern Spain). *J. Hum. Evol.* **65**, 457–464 (2013).

31. M. C. Langley, P. S. C. Taçon, The age of Australian rock art: A review. *Aust. Archaeol.* **71**, 70–73 (2010).

32. K. L. Steelman, F. C. Ramírez, R. F. Valcarce, T. Guilderson, M. W. Rowe, Direct radiocarbon dating of megalithic paints from north-west Iberia. *Antiquity*. **79**, 379–389 (2005).

33. A. I. Thackeray, Dating the rock art of southern Africa. *Goodwin Ser.* **4**, 21–26 (1983).

34. R. G. Bednarik, G. Kumar, A. Watchman, R. G. Roberts, Preliminary results of the EIP Project (2005) (available at http://ro.uow.edu.au/scipapers/3611/).

35. A. D. Mazel, A. L. Watchman, Dating rock paintings in the uKhahlamba-Drakensberg and the Biggarsberg, KwaZulu-Natal, South Africa. *South. Afr. Humanit.* **15**, 59–73 (2003).

36. J. E. Francis, L. L. Loendorf, R. I. Dorn, AMS radiocarbon and cation-ratio dating of rock art in the Bighorn Basin of Wyoming and Montana. *Am. Antiq.* **58**, 711–737 (1993).

37. P. S. Taçon, N. Boivin, M. Petraglia, J. Blinkhorn, A. Chivas, R. G. Roberts, D. Fink, T. Higham, P. Ditchfield, R. Korisettar, others, Mid-Holocene age obtained for nested diamond pattern petroglyph in the Billasurgam Cave complex, Kurnool District, southern India. *J. Archaeol. Sci.* **40**, 1787–1796 (2013).

38. A. Watchman, N. Cole, Accelerator radiocarbon dating of plant-fibre binders in rock paintings from northeastern Australia. *Antiquity*. **67**, 355–358 (1993).

39. R. Bendrey, Review of Wadi Sura–The Cave of Beasts edited by Rudolph Kuper. *Pastoralism*. **4**, 2 (2014).

40. H. Valladas, J. Clottes, J.-M. Geneste, M. A. Garcia, M. Arnold, H. Cachier, N. Tisnérat-Laborde, Palaeolithic paintings: Evolution of prehistoric cave art. *Nat. Lond.* **413**, 479 (2001).

41. A. W. G. Pike, D. L. Hoffmann, M. García-Diez, P. B. Pettitt, J. Alcolea, R. D. Balbín, C. González-Sainz, C. de las Heras, J. A. Lasheras, R. Montes, J. Zilhão, U-series dating of paleolithic art in 11 caves in Spain. *Science*. **336**, 1409–1413 (2012).

42. H. Valladas, H. Cachier, et al, Direct radiocarbon dates for prehistoric paintings at the Altamira, El Castillo and Niaux caves. *Nat. Lond.* **357**, 68 (1992).

43. H. Valladas, N. Tisnérat-Laborde, H. Cachier, M. Arnold, F. B. de Quirós, V. Cabrera-Valdés, J. Clottes, J. Courtin, J. J. Fortea-Pérez, C. Gonzáles-Sainz, A. Moure-Romanillo, Radiocarbon AMS Dates for paleolithic cave paintings. *Radiocarbon*. **43**, 977–986 (2001).

44. K. W. Butzer, G. J. Fock, L. Scott, R. Stuckenrath, Dating and context of rock engravings in southern Africa. *Science*. **203**, 1201–1214 (1979).

45. Z. Zorich, From the Trenches - Drawing Paleolithic Romania - Archaeology Magazine Archive, (available at http://archive.archaeology.org/1201/trenches/coliboaia_cave_romania_charcoal_drawings.html).

46. D. Huyge, A. Watchman, M. De Dapper, E. Marchi, Dating Egypt's oldest 'art': AMS 14C age determinations of rock varnishes covering petroglyphs at El-Hosh (Upper Egypt). *Antiquity*. **75**, 68–72 (2001).

47. N. Mercier, H. Valladas, T. Aubry, J. Zilhão, J. L. Jorons, J.-L. Reyss, F. Sellami, Fariseu: first confirmed open-air palaeolithic parietal art site in the Côa Valley (Portugal). *Antiquity*. **80** (2006) (available at http://www.antiquity.ac.uk/projgall/mercier/).

48. C. Sand, H. Valladas, H. Cachier, N. Tisnérat-Laborde, M. Arnold, J. Bolé, A. Ouetcho, Oceanic rock art: first direct dating of prehistoric stencils and paintings from New Caledonia (Southern Melanesia). *Antiquity*. **80**, 523–529 (2006).

49. A. Watchman, A review of the theory and assumptions in the AMS dating of the Foz Côa petroglyphs, Portugal. *Rock Art Res.* **13**, 21–29 (1996).

50. A. Moure Romanillo, M. Gonzalez Morales, Datation 14C d'une zone décorée de la grotte Fuente del Salin. *Int. Newsl. Rock Art - INORA* (1992).

51. J. Clottes, H. Valladas, H. Cachier, M. Arnold, Des dates pour Niaux et Gargas. *Bull. Société Préhistorique Fr.* **89**, 270–274 (1992).

52. P. R. Geib, H. C. Fairley, Radiocarbon Dating of Fremont Anthropomorphic Rock Art in Glen Canyon, South-central Utah. *J. Field Archaeol.* **19**, 155–168 (1992).

53. H. Valladas, E. Kaltnecker, A. Quiles, N. Tisnérat-Laborde, D. Genty, M. Arnold, E. Delqué-Količ, C. Moreau, D. Baffier, J. J. C. Merle, J. Clottes, M. Girard, J. Monney, R. Montes, C. Sainz, J. L. Sanchidrian, R. Simonnet, Dating French and Spanish prehistoric decorated caves in their archaeological contexts. *Radiocarbon*. **55**, 1422–1431 (2013).

54. A. Broglio, M. De Stefani, F. Gurioli, P. Pallecchi, G. Giachi, T. Higham, F. Brock, L'art aurignacien dans la décoration de la Grotte de Fumane. *L'Anthropologie*. **113**, 753–761 (2009).

55. P. Ambert, J.-L. Guendon, P. Galant, Y. Quinif, A. Gruneisen, A. Colomer, D. Dainat, B. Beaumes, C. Requirand, Attribution des gravures paléolithiques de la grotte d'Aldène (Cesseras, Hérault) à l'Aurignacien par la datation des remplissages géologiques. */data/revues/16310683/00040003/04001691/* (available at http://www.em-consulte.com/en/article/30133).

56. J. Jaubert, D. Genty, H. Valladas, H. Camus, P. Courtaud, C. Ferrier, V. Feruglio, N. Fourment, S. Konik, S. Villotte, C. Bourdier, S. Costamagno, M. Delluc, N. Goutas, É. Katnecker, L. Klaric, M. Langlais, L. Ledoux, F. Maksud, M. O'Farrell, J.-B. Mallye, M. Pierre, E. Pons-Branchu, É. Régnier, I. Théry-Parisot, The chronology of human and animal

presence in the decorated and sepulchral cave of Cussac (France). *Quat. Int.* **432**, 5–24 (2017).

57. V. Plagnes, C. Causse, M. Fontugne, H. Valladas, J.-M. Chazine, L.-H. Fage, Cross dating (Th/U-14 C) of calcite covering prehistoric paintings in Borneo. *Quat. Res.* **60**, 172–179 (2003).

58. D. E. Nelson, G. Chaloupka, C. Chippindale, M. S. Alderson, J. R. Southon, Radiocarbon dates for beeswax figures in the prehistoric rock art of Northern Australia. *Archaeometry*. **37**, 151–156 (1995).

59. K. L. Steelman, M. W. Rowe, V. N. Shirokov, J. R. Southon, Radiocarbon dates for pictographs in Ignatievskaya Cave, Russia: Holocene age for supposed Pleistocene fauna. *Antiquity*. **76**, 341–348 (2002).

60. P. S. Taçon, M. Aubert, L. Gang, Y. Decong, L. Hong, S. K. May, S. Fallon, J. Xueping, D. Curnoe, A. I. Herries, Uranium-series age estimates for rock art in southwest China. *J. Archaeol. Sci.* **39**, 492–499 (2012).

61. E. Stasack, R. I. Dorn, G. Lee, First direct 14C ages on Hawaiian petroglyphs. *Asian Perspect.* **35**, 51–72 (1996).

62. V. E. Shchelinsky, Some results of new investigations at the Kapova Cave in the southern Urals. *Proc. Prehist. Soc.* **55**, 181–191 (1989).

63. W. A. Neves, A. G. M. Araujo, D. V. Bernardo, R. Kipnis, J. K. Feathers, Rock art at the pleistocene/holocene boundary in eastern South America. *PLoS ONE*. **7**, e32228 (2012).

64. S. O'Connor, K. Aplin, E. S. Pierre, Y. Feng, Faces of the ancestors revealed: discovery and dating of a Pleistocene-age petroglyph in Lene Hara Cave, East Timor. *Antiquity*. **84**, 649–665 (2010).

65. J. Russ, M. Hyman, M. Rowe, Direct radiocarbon dating of rock art. *Radiocarbon*. **34**, 867–872 (1992).

66. S. di Lernia, M. Gallinaro, The date and context of neolithic rock art in the Sahara: engravings and ceremonial monuments from Messak Settafet (south-west Libya). *Antiquity*. **84**, 954–975 (2010).

67. A. D. Mazel, A. L. Watchman, Accelerator radiocarbon dating of Natal Drakensberg paintings: results and implications. *Antiquity*. **71**, 445–449 (1997).

68. B. David, B. Barker, F. Petchey, J.-J. Delannoy, J.-M. Geneste, C. Rowe, M. Eccleston, L. Lamb, R. Whear, A 28,000 year old excavated painted rock from Nawarla Gabarnmang, northern Australia. *J. Archaeol. Sci.* **40**, 2493–2501 (2013).

69. M. S. Corchón Rodríguez, H. Valladas, J. Bécares Pérez, M. Arnold, N. Tisnerat, H. Cachier, Datación de las pinturas y revisión del Arte Paleolítico de Cueva Palomera (Ojo Guareña, Burgos, España) (2009) (available at https://gredos.usal.es/jspui/handle/10366/70469).

70. U. A. Thaw, The "neolithic" culture of the Padah-lin Caves. *Asian Perspect.* **14**, 123–133 (1971).

71. A. C. Roosevelt, M. Lima da Costa, C. Lopes Machado, M. Michab, N. Mercier, H. Valladas, J. Feathers, W. Barnett, M. Imazio da Silveira, A. Henderson, others, Paleoindian cave dwellers in the Amazon: the peopling of the Americas. *Sci.-N. Y. THEN Wash.*-, 373–384 (1996).

72. K. Mulvaney, Dating the Dreaming: extinct fauna in the petroglyphs of the Pilbara region, Western Australia. *Archaeol. Ocean.* **44**, 40–48 (2009).

73. G. Sauvet, À la recherche du temps perdu. Méthodes de datations en art préhistorique (available at https://www.researchgate.net/profile/Georges_Sauvet2/publication/289376793_A_la_recherche_du_temps_perdu_methodes_de_datations_en_art_prehistorique_L'exemple_des_sites_aurignaciens/links/568c0e1f08ae197e42689524.pdf).

74. D. Huyge, D. A. Vandenberghe, M. De Dapper, F. Mees, W. Claes, J. C. Darnell, First evidence of Pleistocene rock art in North Africa: securing the age of the Qurta petroglyphs (Egypt) through OSL dating. *Antiquity*. **85**, 1184–1193 (2011).

75. A. W. G. Pike, M. Gilmour, P. Pettitt, R. Jacobi, S. Ripoll, P. Bahn, F. Muñoz, Verification of the age of the Palaeolithic cave art at Creswell Crags, UK. *J. Archaeol. Sci.* **32**, 1649–1655.

76. A. Bonneau, F. Brock, T. Higham, D. G. Pearce, A. M. Pollard, An improved pretreatment protocol for radiocarbon dating black pigments in San rock art. *Radiocarbon*. **53**, 419–428 (2011).

77. N. Cole, A. Watchman, AMS dating of rock art in the Laura Region, Cape York Peninsula, Australia–protocols and results of recent research. *Antiquity*. **79**, 661–678 (2005).

78. M. Fontugne, Q. Shao, N. Frank, F. Thil, N. Guidon, E. Boeda, Cross-Dating (Th/U-14 C) of Calcite Covering Prehistoric Paintings at Serra da Capivara National Park, Piaui, Brazil. *Radiocarbon*. **55**, 1191–1198 (2013).

79. A. Jerardino, N. Swanepoel, Painted Slabs from Steenbokfontein Cave: The Oldest Known Parietal Art in Southern Africa. *Curr. Anthropol.* **40**, 542–547 (1999).

80. M. Aubert, A. Brumm, M. Ramli, T. Sutikna, E. W. Saptomo, B. Hakim, M. vd Morwood, G. D. van den Bergh, L. Kinsley, A. Dosseto, Pleistocene cave art from Sulawesi, Indonesia. *Nature*. **514**, 223 (2014).

81. M. Hachid, J.-L. Le Quellec, A. Amara, L. Beck, A. Heddouche, E. Kaltnecker, S. Lahlil, S. Merzoug, C. Moreau, A. Quiles, others, Quelques résultats du projet de datation directe et indirecte de l'art rupestre saharien. *Signs Which Times*, 71–96 (2012).

82. J. F. Simek, A. Cressler, N. P. Herrmann, S. C. Sherwood, Sacred landscapes of the south-eastern USA: prehistoric rock and cave art in Tennessee. *Antiquity*. **87**, 430–446 (2013).

83. R. G. Bednarik, in *Proceedings of the IFRAO Congress* (2010; http://www.ifrao.com/wp-content/uploads/2015/08/12Asia2.pdf).

84. R. I. Dorn, P. B. Clarkson, M. F. Nobbs, L. L. Loendorf, D. S. Whitley, New Approach to the Radiocarbon Dating of Rock Varnish, with Examples from Drylands. *Ann. Assoc. Am. Geogr.* **82**, 136–151 (1992).

85. L. V. Benson, E. M. Hattori, J. Southon, B. Aleck, Dating North America's oldest petroglyphs, Winnemucca Lake subbasin, Nevada. *J. Archaeol. Sci.* **40**, 4466–4476 (2013).

86. A. I. Thackeray, J. F. Thackeray, P. B. Beaumont, J. C. Vogel, Dated rock engravings from Wonderwerk Cave, South Africa. *Science*. **214**, 64–67 (1981).

Acknowledgements

The idea of testing our model on the case of parietal rock art emerged from a meeting at University College, London, between Richard Walker, Stephen Shennan & Mark Thomas (University College, London) and Anders Eriksson. Population estimates were kindly contributed by Axel Timmermann, International Pacific Research Center, University of Hawaii. Michelle Langley, Griffith University, Brisbane, Australia; Australian National University, Canberra, Australia, kindly contributed data from a published survey of Australian rock art. Werner van Geit, Blue Brain Project, EPFL, Switzerland, contributed important code fragments. Isabel Marquez cross-checked the data for rock art sites. Mark Thomas and Stephan Shennan, Michael Herzog (EPFL Switzerland), Ruedi Füschlin (ZHAW, Switzerland), and Lenwood Heath (Virginia Tech) reviewed earlier versions of this manuscript, providing valuable feedback. Henry Markram, leader of the Blue Brain Project, provided vital encouragement and support.

Author contributions

RW developed the original epidemiological model and wrote a prototype version of the software. AE contributed the population data used in the analysis, substantially contributed to the development of the epidemiological model, and developed the concepts and analysis tools used to validate the model. RW and AE jointly wrote the manuscript. CR rewrote the prototype data extraction and analysis software from RW and AE, and developed the publication version of the tool TH contributed to the formal derivation of the epidemiological model. FC contributed to the statistical analysis.

Figures

Fig. 1

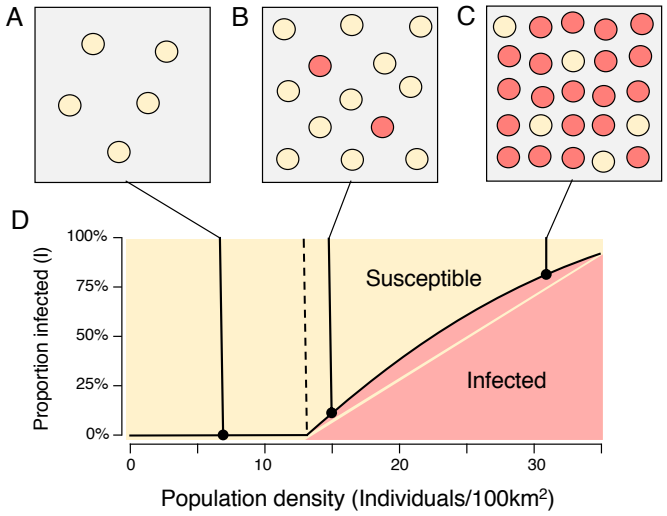

Fig. 1: As population density increases opportunities for transmission between subpopulations also increase. **A:** Below the critical threshold ρ^*, the innovation cannot spread between subpopulations. **B-C:** Above the critical threshold the proportion of infected subpopulations is an increasing function of population density.

Fig. 2

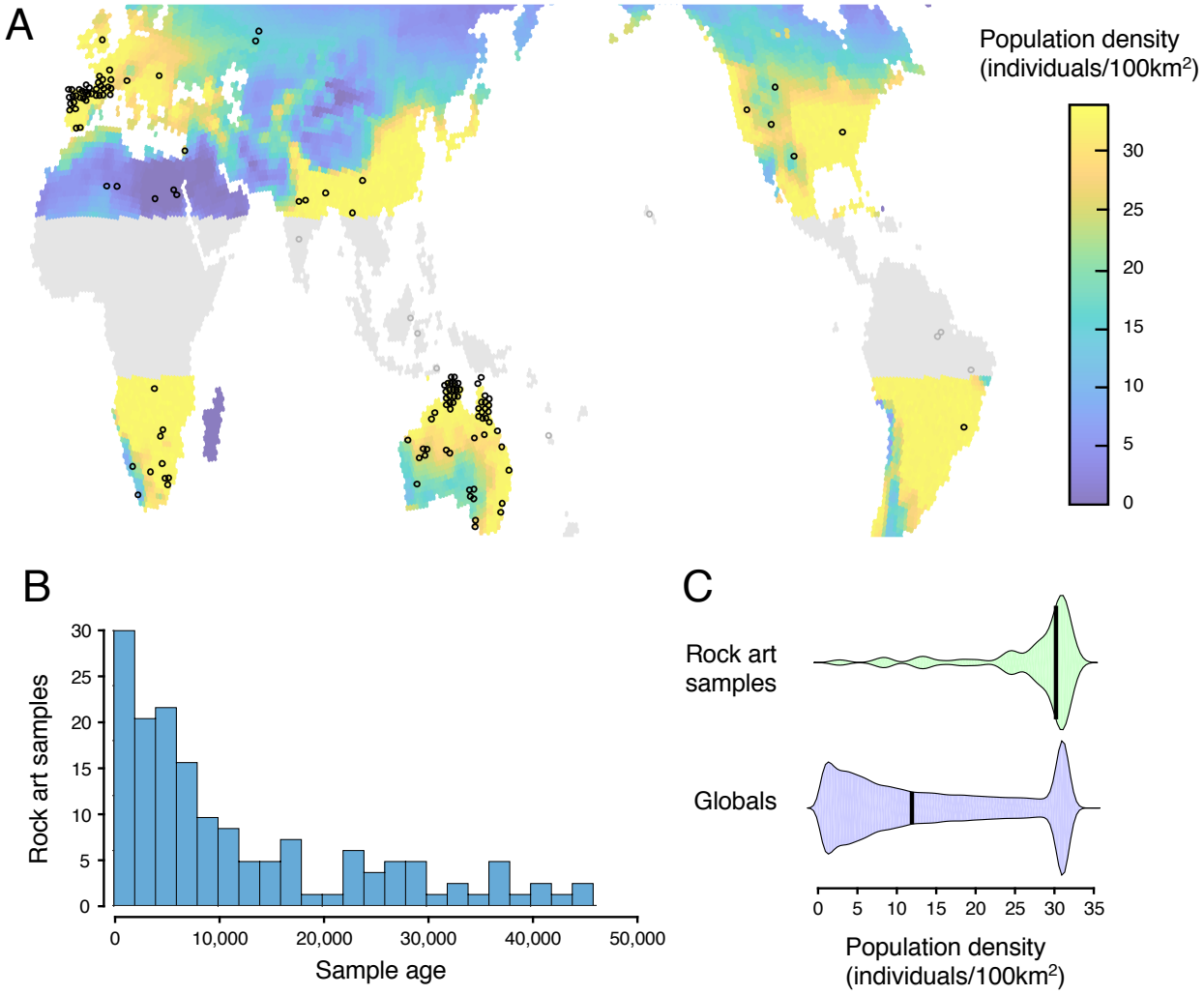

Fig. 2: Distribution of rock art sites in the rock art dataset (133 sites)**. A:** Geographical distribution of sites and inferred population distributions (maximum value over the last 46,000 years, see color bar for scale; areas excluded from the analysis shown in grey). **B:** distribution by earliest date of rock art at site location **C:** comparison of population densities for all sites vs. all globals.

Fig. 3

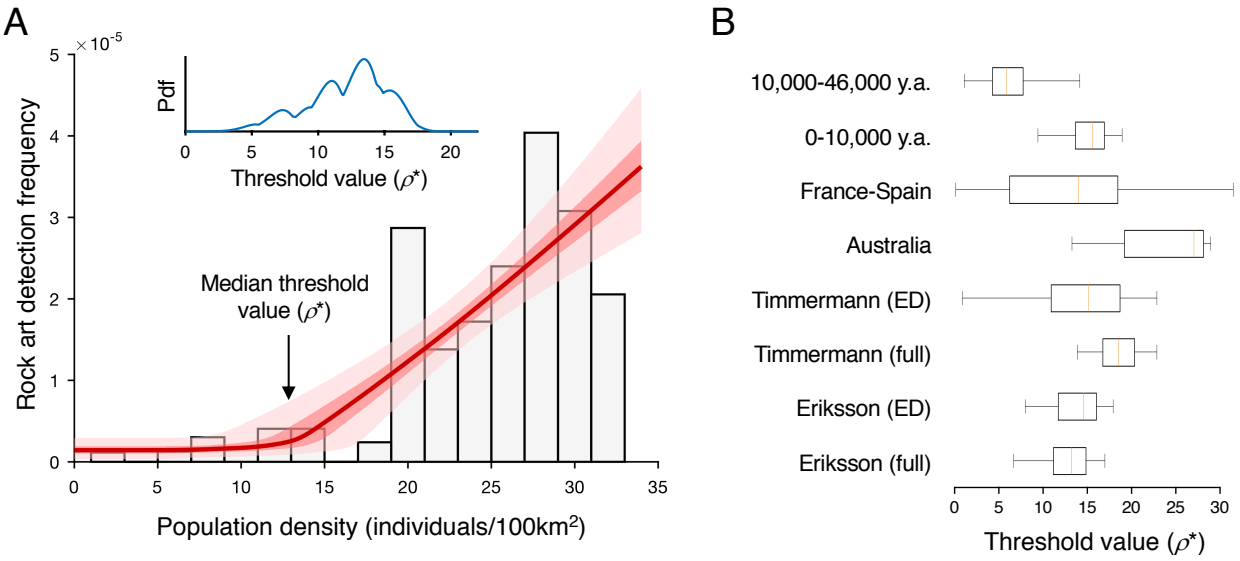

Fig. 3: A. Inferred detection frequencies given the epidemiological model, the full archaeological dataset, and the population estimates in (*24*, *25*). Grey bars: empirical frequencies of rock art in different intervals of population density. Red line: estimated rock art detection rate as a function of population density (median of posterior distribution of estimated detection rate, with interquartile range in dark pink and 95% CI in pale pink). Also shown is the posterior probability density function (pdf) of the threshold value (ρ^*, inset); the median value of this distribution is indicated by an arrow on the main axis. **B.** Inferred values of the critical threshold for the different analyses described in the paper (ED: exact direct; orange line: maximum likelihood estimate; box: interquartile range; whiskers: CI 0.025-0.975).

Supplementary Materials

Materials and Methods

Derivation of the model

The model describes the diffusion of a cultural innovation (e.g. a new behavior, a new skill, a technological invention, a new belief) through a Culturally Effective Population (CEP) (*9*) i.e. a closed network of communicating nodes, where nodes can be individuals or groups of individuals (subpopulations). Here they are subpopulations. Notation for the disease dynamics follows (*22*).

Assume a stable CEP of size N. Let the population be divided into I *infected*, and S uninfected, *susceptible* subpopulations. Thus:

$$\mathrm{N} = I + S \tag{1}$$

For convenience, consider I and S as the proportion of infected and susceptible subpopulations

$$\text{i.e. } \mathrm{I} + \mathrm{S} = 1 \tag{2}$$

If the population is "well mixed" (i.e. all subpopulations are in social contact), any susceptible subpopulation can acquire the innovation from any infected subpopulation. Let β be the rate of transmission per time step and γ the rate of recovery (the rate at which infected populations lose the ability to produce rock art). Thus, the rate of change in the proportion of infected subpopulations is given by

$$\frac{dI}{dt} = \beta\mathrm{IS} - \gamma\mathrm{I} \tag{3}$$

In a partially connected population, the only subpopulations to which an infected subpopulation can transmit an innovation are the susceptible subpopulations with which it is in contact. Let k_s be the mean number of susceptible contacts for each infected subpopulation, determined by the proportion of susceptible subpopulation in the population, S multiplied by k. i.e.

$$k_s = k\mathrm{S} \tag{4}$$

Substituting for S in equation (3) and combining with equation (1) we obtain:

$$\frac{dI}{dt} = \beta Ik(1-I) - \gamma I \tag{5}$$

Rearranging, solving for $\frac{dI}{dt} = 0$, and imposing $I^* \geq 0$, we obtain the final size of the infected subpopulations:

$$I^* = \begin{cases} 0, \ 1 - \frac{\gamma}{k\beta} \leq 0 \\ \left(1 - \frac{\lambda}{k\beta}\right), 1 - \frac{\gamma}{k\beta} > 0 \end{cases} \tag{6}$$

If social contact numbers k are proportional to the square root of density (*23*), i.e. k=$\alpha\sqrt{\rho}$,

$$\mathrm{I}^* = \begin{cases} 0, \rho \leq \frac{\gamma}{\alpha\beta\sqrt{p}} \\ 1 - \frac{\gamma}{\alpha\beta\sqrt{p}}, \rho > \frac{\gamma}{\alpha\beta\sqrt{p}} \end{cases} \tag{7}$$

Setting α and β to 1, we obtain

$$I^* = \begin{cases} 0, \rho \leq \frac{\gamma}{\sqrt{p}} \\ 1 - \frac{\gamma}{\sqrt{p}}, \rho > \frac{\gamma}{\sqrt{p}} \end{cases} \quad (8)$$

In short, there exists a critical population density, ρ^*, such that at all densities below ρ^* there are no infected subpopulations , and at all densities beyond ρ^*, the number of infected individuals is greater than zero.

At ρ^*, $\rho - \frac{\gamma\sqrt{p}}{\alpha\beta} = 0$. Thus:

$$\rho^* = \gamma^2 \quad (9)$$

Finally, if each infected subpopulation has an equal probability, z, of producing an artifact that is later recorded in the archaeological record, the probability P, that the n infected subpopulations will generate at least one such trace, is given by:

$$P = (1-(1 - zI^*)^n) \quad (10)$$

Since zI^* is small

$$P \cong zI^{*}n \tag{11}$$

The value of n for a cell of standard area, with standard mean community size, is proportional to the population density for the cell.

$$n = \mu\rho \tag{12}$$

Grouping μ and z in a single variable ζ we obtain

$$P \cong \zeta\, I^{*}\rho \tag{13}$$

In the setting of our empirical study, inferred population sizes may contain large errors, especially when sites dates are minimum dates or indirect estimates. We, therefore, include an error term ε.

$$P = \zeta\,(1-\varepsilon)p_i\rho\; +\; \varepsilon \tag{14}$$

This is the model we tested in our empirical study.

Rock art dataset

The analysis presented here is based on a dataset of parietal rock art, generated through a literature search with Google Scholar. We are aware that the database contains only a small proportion of all rock painting sites in the world, and that it may be subject to systematic biases. These are discussed in the main body of our paper.

For the purposes of our survey, parietal rock art was defined to include all figurative and non-figurative pictograms (paintings and drawings) and petroglyphs (engravings) using rock wall as a canvas. “Art mobilier” (e.g. figurines) and geoglyphs (i.e. large designs or motifs on the ground) were excluded from the analysis.

The survey was seeded using the query:
("rock art" OR "parietal art" OR petroglyphs OR pictographs) [AND] (radiocarbon OR AMS OR luminescence OR Uranium).

We read the top 300 articles found by the query that were accessible through the EPFL online library, together with other relevant papers, cited within these articles. Sites where drawings, paintings and engravings were reported, were systematically recorded. Sites with no radiocarbon, optical luminescence or Uranium-thorium date were excluded.

For each dated site, we recorded the longitude and latitude of the site (where reported), its name, the earliest and latest dates of “art” found at the site (converted to years before 1950 or years BP), the name of the modern country where the site was located, the journal reference, the method(s) used to produce the date, the nature of the dating procedure (direct dating, indirect dating), the nature of the data provided (exact data, minimum date, maximum date, mixed) a descriptor of the artefacts found (paintings, drawings, petroglyphs etc.), and a flag showing disputed dates. Where

different authors reported different dates for a site, without disputing dates proposed by other authors, we systematically used the dates from the most recent report.

In cases where the article did not provide a latitude and longitude, online resources were used to locate the information. The main such resources were D. Zwiefelhofer's FindLatitudeAndLongitude web site (https://www.findlatitudeandlongitude.com/) , which is based on Google Maps, and Austarch, a database of 14C and Luminescence Ages from Archaeological Sites in Australia, managed by A. Williams and Sean Ulm (*19*).

The survey generated 190 records. Merging of records with the identical latitudes and longitudes and overlapping dates (5 records eliminated), and exclusion of duplicate records (12), modern sites (1), sites which did not meet the inclusion criteria (13), sites where the source was deemed unreliable (5), sites where reliable geographical coordinates were unavailable (12), sites with disputed or doubtful dates (8) and 1 site described in a retracted article, left a total of 133 records.

All except 5 of these records referred to sites located between 20°- 60°N and 10° - 40°S. Since, our data analysis (see below) compares the distribution of population densities for "sites" against the distribution of "globals" defined as all cells, within a comparable range of dates and latitudes, inclusion of these sites would have required the inclusion of a large number of globals at the same latitudes, potentially distorting the results of the analysis. They were therefore excluded from the

subsequent analysis. For similar reasons, one very early site (Blombos Cave, South Africa) (77,000 years ago) was also excluded.

After these exclusions the final dataset consisted of 127 records. During the analysis phase, it was found that 8 records referred to sites with estimated population densities less than 1 individual / 100km^2 or no estimated population at the date corresponding to the earliest rock art at the site. These sites were not considered in the later phases of the analysis.

Estimates of population density

The population density estimates used in our paper combine results from a climate-informed spatial genetic model (*24*) with an improved climate model in (*25*). Briefly, models combine climate estimates for the last 120,000 years, based on the Hadley Centre model HadCM3, with data on patterns of modern genetic variability from the human genome diversity panel-Centre d'Etude du Polymorphisme Humain (HGDP-CEPH), and a mathematical model of local population expansion and dispersal. Estimates of past precipitation and temperature are used to estimate Net Primary Productivity (NPP), and hence maximum human carrying capacity, for each cell in a hexagonal lattice with equal area cells 100 km wide, for all dates from 120,000 years ago to the present using time steps of 25 years. The carrying capacity is a continuous function of NPP governed by two NPP threshold values and a maximum carrying capacity parameter, K. The carrying capacity is zero below the lower NPP threshold, increase linearly from zero to K between the two NPP thresholds, and is constant and equal to K for NPP above the upper NPP threshold value. Human expansion out of Africa is simulated using a model where populations that have reached the maximum carrying capacity of a cell expand into neighboring cells. Approximate Bayesian Computing is used to compare models with a broad range of parameter values and

starting values. Model evaluation is based on their ability to predict regional estimates of pairwise time to most recent common ancestor (TRMCA). We generated population size estimates using parameters from the high-ranking scenario described in Fig. 2 and Movie S1 in (*24*) and NPP values from (*25*) as these contain a more accurate model of the American ice sheet dynamics and therefore give more accurate estimates of the colonization of the Americas by humans.

These population estimates were compared against the results using a second set of population estimates reported in (*26*). The data refer to the scenario A (early exit) scenario described in the paper. As in (*24*), human population density estimates are based on a climate model (LOVECLIM) combined with a reaction-diffusion Human Dispersal Model. Unlike the model in (*24*), the estimates do not take account of genetic data. A second difference concerns the population estimator, which is based not just on NPP but also on temperature and predicted "desert faction" and incorporates *ad hoc* modeling hypotheses absent in the previous model. These include accelerated human dispersal along coastlines ("a coastal express") and a special Gaussian decay function, modeling the probability of island hopping as a function of distance.

For clarity of presentation the outputs from both models are expressed in terms of effective population/ 100km^2.

Data analysis

In many sites in our dataset, the rock art reported in the literature spanned a broad range of dates. For the purposes of our analysis, we considered only the *oldest* date for each site. This procedure reduced our sample size and the statistical power of our analysis, but also the risk of artefacts due to dependencies in the data. Where confidence intervals were given, we used the midpoint of the

interval. Each site was associated with the estimated population density for the cell in the population model whose date and center point were closest to the date and location of the site. Globals were defined according to the needs of the individual analysis

Analysis	Definition of globals
World	All cells with non-zero population with dates in the range 0-46,000 years ago and locations between 60°N and 20°N or between 10°S and 40°S
Periods	(1) All cells with non-zero population with age between 0 and 9999 years. (2) All cells with non-zero population with age between 10000 and 46000 years.
France and Spain	Derived from the maximum and minimum latitudes and longitudes for sites in our dataset with locations in modern France or Spain. All cells with non-zero population lying in a "rectangle" with NW corner (lat: 50.84°N, lon: 10°) and SE corner (lat: 35.00°N, lon 7.00°E)

Australia	Derived from the maximum and minimum latitudes and longitudes for sites in our dataset with locations in modern Australia. All cells with non-zero population lying in a "rectangle" with NW corner (lat: 25.27°S, lon: 133.77°E) and SE corner (lat: 39.16°S, lon: 154.86E)

Data for sites and globals were binned by population density (one bin for each unit of density in the original data). Numbers of sites and globals and frequency of sites (sites/globals) were computed for each bin

Testing model predictions

The likelihood of the model, given the observed ratio of sites to globals at different population densities, was tested for discrete plausible values of the γ, ζ and ε parameters. The transmission rate τ was set to 1. The model with the highest likelihood was compared against the likelihood of the most likely constant model $z(\rho) = k$ and the most likely proportional model $z(\rho) = \beta\rho$. The value of the threshold was inferred inserting the most likely inferred values of γ and ζ in the model

$$\rho^* = \left(\frac{\gamma}{\tau}\right)^2 \quad (15)$$

Analysis by period and geographical area

Subsets of "sites" and "globals" belonging to specific date bands (0 - 9999 years ago, 10000-46000 years ago) and specific geographical areas with high numbers of sites (France/Spain, Australia) were subjected to the same analyses applied to the full dataset (see above).

Software

Data extraction and analysis was based on custom code written in Python 2.7, using the Anaconda development environment.

Software availability

Python source code for the software used to perform the analyses is available under a GPL 3.0 license, at https://github.com/rwalker1501/cultural_epidemiology.git.

The software includes (i) the script used to generate the figures and tables shown in this paper; (ii) methods to run additional data analyses and to produce figures not shown in the paper; (iii) a menu driven program providing easy to use access to these functions (iv) documented source code for the statistical calculations and plots used in the paper and the additional analyses

Data

The GIT repository includes the full rock art database used for the analysis, and copies of the population estimates from the Timmermann and the Eriksson models.

The original population estimates from Eriksson can be found at: https://osf.io/dafr2/

The original population estimates from Timmermann can be found at https://climatedata.ibs.re.kr/grav/data/human-dispersal-simulation

Supplementary Figures

Fig. S1

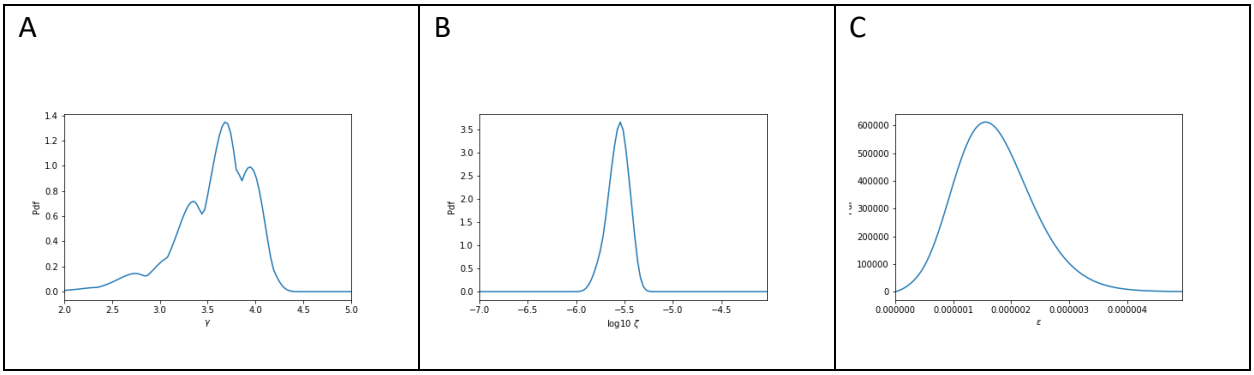

Fig. S1: Posterior distributions for the γ, ξ, and ε parameters for the epidemiological model as shown in Fig. 3A (observed site detection rates, for the full archaeological dataset and the combined population estimates in (*24*, *25*))

,

Fig. S2

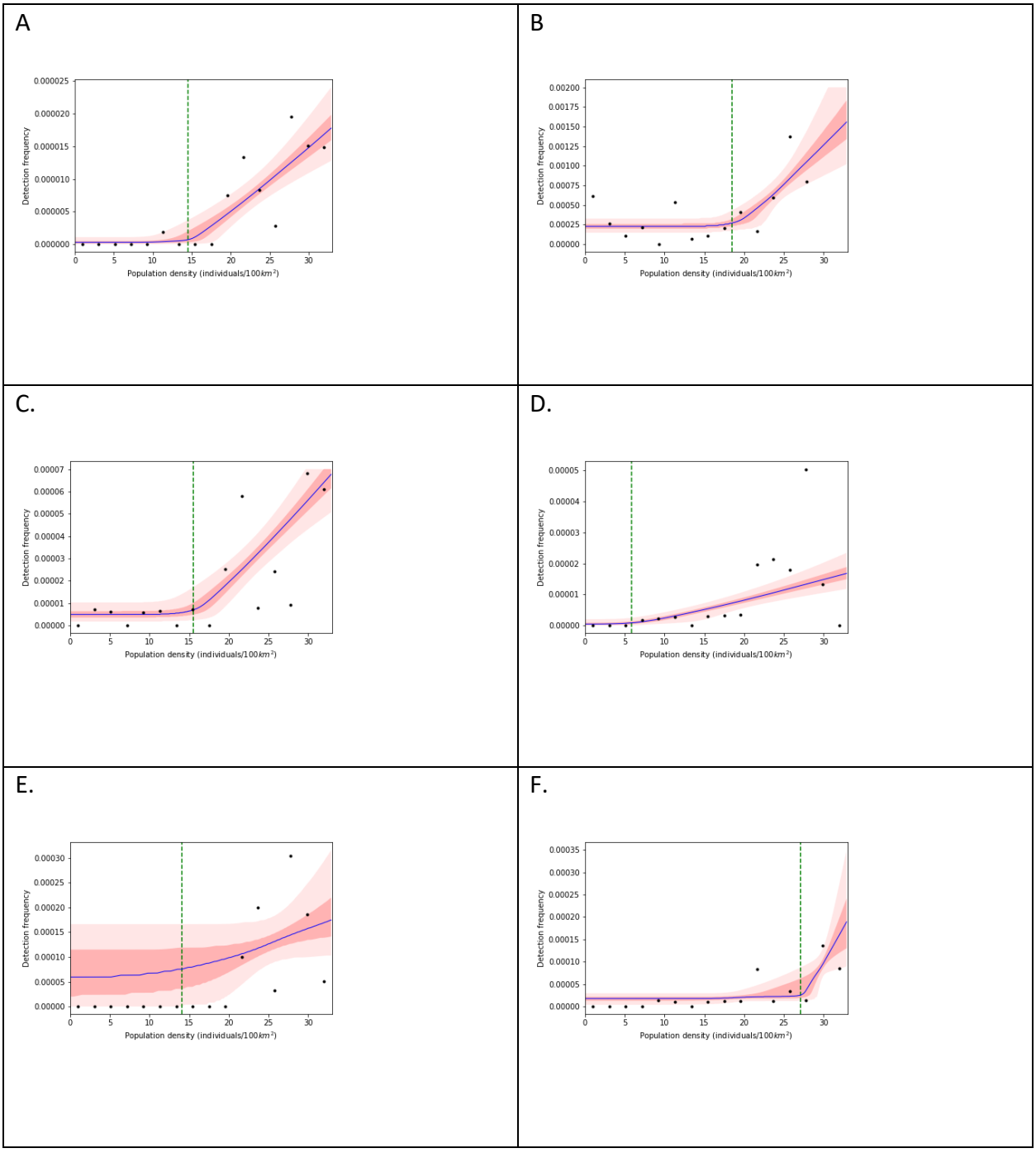

Fig. S2: **A.** Inferred detection frequencies given the epidemiological model, a filtered version of the archaeological dataset using only sites with exact dates obtained with direct methods , and the population estimates in (*24*, *25*). **B.** Inferred detection frequencies, using the alternative population estimates in (*26*). **C.** Inferred detection frequencies, using only sites with dates between 0 and 9999 years ago, and the population estimates in (*24*, *25*). **D.** As in C, using only sites with dates older than 9999 years ago. **E.** As in D using only sites located in modern France and Spain. **F.** As in E using only sites located in modern Australia.

Supplementary Material data

Supplementary Table 1: rock art dataset

See attached file "SM Table 1 - Rock Art Dataset.csv"

Supplementary Table 2: Detailed results from analyses in paper

See attached file " SM Table 2 - Table of Results.pdf"